Available online at www.sciencedirect.com

ScienceDirect

Procedia Manufacturing 26 (2018) 173–180

Procedia MANUFACTURING

www.elsevier.com/locate/procedia

46th SME North American Manufacturing Research Conference, NAMRC 46, Texas, USA

Receptance coupling model for variable dynamics in fixed-free thin rib machining

Andrew Honeycutt, Tony Schmitz*

UNC Charlotte, Mechanical Engineering and Engineering Science, Charlotte, NC 28223, USA

* Corresponding author. Tel.: +1-704-687-5086.
E-mail address: tony.schmitz@uncc.edu

Abstract

An analytical approach for predicting thin rib, fixed-free beam dynamics with varying geometries is presented. The proposed method uses receptance coupling substructure analysis (RCSA) to predict the stepped thickness beam receptances (or frequency response functions) at the fixed-free beam's free end and at the change in thickness. The assembly receptances are calculated by rigidly connecting receptances that describe the individual stepped beam sections, where the section receptances are computed using the Timoshenko beam model. Comparisons with finite element calculations are completed to verify the technique. It is observed that the RCSA predictions agree closely with finite element results. Experiments are also performed, where the stepped beam thickness is changed by multiple machining passes, and receptance measurements are carried out between passes. The RCSA predictions are compared to experimental results for natural frequency and stiffness. Agreement in natural frequency to within two percent is reported.

Peer-review under responsibility of the scientific committee of the 4th International Conference on System-Integrated Intelligence.

Keywords: Dynamics; beam; rib; milling; receptance coupling

1. Introduction

It is common practice to produce monolithic metallic components with thin ribs from solid billets by machining (subtractive manufacturing). This enables complex parts with high strength-to-weight ratio to be produced without significant assembly time and cost. Application domains range from aerospace structures to laptop cases. With the recent advances in metal additive manufacturing, it is also possible to produce near net shape parts that require only minimal machining to provide the desired surface finish and dimensional accuracy. This is particularly attractive for titanium alloys due to their

2351-9789
Peer-review under responsibility of the scientific committee of the 4th International Conference on System-Integrated Intelligence.
10.1016/j.promfg.2018.07.024

high material cost and low machinability. The inherent challenge with this hybrid (i.e., combined additive and subtractive) approach is machining flexible parts. The low dynamic stiffness of the thin, near net shape ribs limits both machining stability (i.e., self-excited vibration, or chatter, can occur) and part accuracy (via the surface location errors that can arise from forced vibrations) [1].

Because thin rib machining is widespread, many authors have reported modeling efforts and production strategies with the intent to improve process performance. These efforts are summarized in Table 1. While this review may not be exhaustive, it does demonstrate the significant effort that has been expended on this important technological challenge over the past two decades.

Table 1. Prior research in thin rib machining.

First author	Year	Ref.	Topic
Y. Altintas	1995	2	The authors considered the influence of plate dynamics on the geometric accuracy of machined thin ribs.
J. Tlusty	1996	3	Techniques for machining thin ribs using relieved shank tooling in a series of axial passes, finishing the rib on every pass, was described.
S. Smith	1998	4	Tool path strategies for the machining of thin webs which rely on the support of the unmachined workpiece were investigated.
H. Ning	2003	5	Finite element thin rib part models were used to assess dimensional accuracy during milling.
S. Ratchev	2004	6	Force-induced geometric errors were predicted in thin rib machining using finite element analysis and a voxel-transformation model.
S. Ratchev	2004	7	An adaptive theoretical force-finite element analysis deflection model was used to predict thin rib surface errors during milling.
U. Bravo	2005	8	A three-dimensional stability lobe diagram was presented that considered both the part and tool frequency response functions, as well as the intermediate stages of the rib machining.
S. Ratchev	2005	9	Finite element models were used to predict and compensate force-induced geometric errors in machining of thin rib structures.
V. Thevenot	2006	10	A three-dimensional stability lobe diagram was presented that incorporated the spatial variation in the thin rib dynamics. Modal testing and finite element analysis were used to identify the thin rib frequency response functions.
I. Mañé	2008	11	A spindle-tool finite element model that considered the gyroscopic moment of the spindle rotor and the speed-dependent bearing stiffness was coupled to a finite element model of the thin rib part to predict milling stability.
J.K. Rai	2008	12	A finite element-based milling process plan verification model was presented. The effects of fixturing, operation sequence, tool path, and operating parameters were considered to predict the thin rib part deflections.
S. Seguy	2008	13	The authors examined the relationship between chatter instability and surface roughness for thin rib milling. Finite element models were used to describe the rib dynamics.
O.B. Adetoro	2009	14	Finite element and experimental frequency response functions were used to obtain stable operating parameters for thin rib machining.
W. Chen	2009	15	The authors considered the effect of machining deformation that occurs in the current layer on the nominal cutting depth in the next layer during thin rib milling.
L. Gang	2009	16	Three-dimensional finite element models of a helical tool and a thin titanium alloy (6Al-4V) cantilever were used to predict the cutting deformation during milling.
L. Arnaud	2011	17	Finite element analysis was used to model the part and time domain simulation was used to predict the thin rib machining stability.
R. Izamshaw	2011	18	A combination of finite element and statistical analyses were used to predict part deflection during thin rib machining.
S. Smith	2012	19	Sacrificial structure preforms that support the part during machining, but are not a part of the finished component, were designed and tested.
A. Polishetty	2014	20	The trochoidal milling strategy was used for thin rib machining of titanium alloy 6Al-4V.

In prior work, finite element analysis has been the primary tool to model and predict the thin rib dynamics and, in many cases, the change in the rib dynamics as material is removed. In this paper, an analytical approach is presented to describe the

stiffness and natural frequency of fixed-free beams, as well as the change in stiffness and natural frequency as material is removed by milling. The specific challenge of near net shape machining, where an initially thin rib is machined to produce a thinner rib, is addressed. The advantage of an analytical approach to the system dynamics prediction is that, as the dynamics change, the machining conditions can be selected and updated at less computational expense than a full finite element solution to maximize material removal rate for the current dynamic system. Naturally, these operating parameters change as material is removed (as evidenced by the prior research efforts), so an analytical updating procedure is beneficial.

In this paper, fixed-free beams with stepped profiles are used to represent the thin ribs geometries and subsequent material removal. The paper outline follows. First, the receptance coupling substructure analysis (RCSA) approach is described. It is implemented to rigidly attach the two sections of the rib: a thicker base and thinner free end. This represents the beam geometry as material is removed and a section of the profile changes. The RCSA calculations predict the assembly receptance (or displacement-to-force frequency response function). The fundamental natural frequency and corresponding modal stiffness are extracted from the predicted receptance and comparisons to finite element analysis calculations are presented. Second, the experimental setup and approach are described. Third, a comparison between experiments and RCSA predictions is provided. Fourth, application considerations and conclusions are presented.

2. RCSA

RCSA is a frequency domain, analytical procedure used to couple component receptances in order to predict the assembly receptances [21, 22]. In this work, the free-free receptances for the machined section of the beam are rigidly coupled to the remaining (unmachined) fixed-free section; see Fig. 1, where E is the elastic modulus and I is the second moment of area. Using rigid compatibility and equilibrium conditions, the assembly direct receptances, $H_{11} = \frac{Y_1}{F_1}$ and $H_{22} = \frac{Y_2}{F_2}$, at assembly coordinates Y_1 and Y_2 are written as a function of the component receptances at coordinates 1, $2a$, and $2b$; see [21] for the derivation. The required direct and cross receptances for the free-free (coordinates 1 and $2a$) and fixed-free (coordinate $2b$) components are:

- $h_{11} = \frac{y_1}{f_1}$, $h_{12a} = \frac{y_1}{f_{2a}}$, $h_{2a1} = \frac{y_{2a}}{f_1}$, $h_{2a2a} = \frac{y_{2a}}{f_{2a}}$, and $h_{2b2b} = \frac{y_{2b}}{f_{2b}}$, where y_i is the component displacement and f_j is the (internal) component force
- $l_{11} = \frac{y_1}{m_1}$, $l_{12a} = \frac{y_1}{m_{2a}}$, $l_{2a1} = \frac{y_{2a}}{m_1}$, $l_{2a2a} = \frac{y_{2a}}{m_{2a}}$, and $l_{2b2b} = \frac{y_{2b}}{m_{2b}}$, where m_j is the (internal) component moment
- $n_{11} = \frac{\theta_1}{f_1}$, $n_{12a} = \frac{\theta_1}{f_{2a}}$, $n_{2a1} = \frac{\theta_{2a}}{f_1}$, $n_{2a2a} = \frac{\theta_{2a}}{f_{2a}}$, and $n_{2b2b} = \frac{\theta_{2b}}{f_{2b}}$, where θ_i is the component rotation
- $p_{11} = \frac{\theta_1}{m_1}$, $p_{12a} = \frac{\theta_1}{m_{2a}}$, $p_{2a1} = \frac{\theta_{2a}}{m_1}$, $h_{2a2a} = \frac{\theta_{2a}}{m_{2a}}$, and $p_{2b2b} = \frac{\theta_{2b}}{m_{2b}}$.

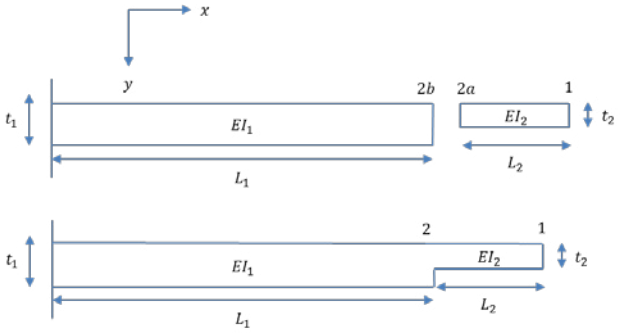

Fig. 1. Beam model for RCSA. (Top) The two components and associated coordinates (1 and $2a$ for the free-free component and $2b$ for the fixed-free component) are identified. (Bottom) The assembly and associated coordinates (1 and 2) are shown.

The assembly receptances are provided in Eqs. 1 and 2 [21].

$$\begin{bmatrix} H_{11} & L_{11} \\ N_{11} & P_{11} \end{bmatrix} = \begin{bmatrix} h_{11} & l_{11} \\ n_{11} & p_{11} \end{bmatrix} - \begin{bmatrix} h_{12a} & l_{12a} \\ n_{12a} & p_{12a} \end{bmatrix} \left(\begin{bmatrix} h_{2a2a} & l_{2a2a} \\ n_{2a2a} & p_{2a2a} \end{bmatrix} + \begin{bmatrix} h_{2b2b} & l_{2b2b} \\ n_{2b2b} & p_{2b2b} \end{bmatrix} \right)^{-1} \begin{bmatrix} h_{2a1} & l_{2a1} \\ n_{2a1} & p_{2a1} \end{bmatrix} \quad (1)$$

$$\begin{bmatrix} H_{22} & L_{22} \\ N_{22} & P_{22} \end{bmatrix} = \begin{bmatrix} h_{2a2a} & l_{2a2a} \\ n_{2a2a} & p_{2a2a} \end{bmatrix} -$$

$$\begin{bmatrix} h_{2a2a} & l_{2a2a} \\ n_{2a2a} & p_{2a2a} \end{bmatrix} \left(\begin{bmatrix} h_{2a2a} & l_{2a2a} \\ n_{2a2a} & p_{2a2a} \end{bmatrix} + \begin{bmatrix} h_{2b2b} & l_{2b2b} \\ n_{2b2b} & p_{2b2b} \end{bmatrix} \right)^{-1} \begin{bmatrix} h_{2a2a} & l_{2a2a} \\ n_{2a2a} & p_{2a2a} \end{bmatrix} \quad (2)$$

The component receptances can be obtained from measurements or models. Two modeling options are the Euler-Bernoulli and Timoshenko beams. In this work, the one-dimensional Timoshenko beam model was implemented to find the free-free receptances. This requires a numerical solution of the partial differential equation displayed in Eq. 3 [23, 24], where ρ is the density, A is the beam's cross-sectional area, E is the elastic modulus, I is the second moment of area, G is the shear modulus, and $\hat{k}$ is a shape factor that depends on the beam's cross section [25]. To determine the required fixed-free receptances for the L_1 section component, the free-free receptances for this component (obtained from Eq. 3) were rigidly coupled to a rigid boundary (i.e., zero receptances). Equation 1 was also applied for this sub-step, where the $2b$ coordinate was assigned to the rigid boundary and the 1 and $2a$ coordinates to the L_1 section component.

$$\left(\frac{\partial^2 y}{\partial t^2} + \frac{EI}{\rho A}\frac{\partial^4 y}{\partial x^4}\right) + \left(\frac{\rho I}{\hat{k}AG}\frac{\partial^4 y}{\partial t^4} + \frac{EI}{\hat{k}AG}\frac{\partial^4 y}{\partial x^2 \partial t^2}\right) - \left(\frac{I}{A}\frac{\partial^4 y}{\partial x^2 \partial t^2}\right) = 0 \quad (3)$$

To provide a numerical validation of the analytical coupling approach, comparisons between the RCSA predictions and ANSYS finite element calculations were completed. Multiple beam geometries (Fig. 1) were tested where the beam thickness was reduced over a varying length, L_2. In each case, the natural frequency and modal stiffness were extracted by peak picking from the direct receptances. Natural frequency, f_n, results are presented in Table 2 and Fig. 2, where the steel beam's elastic modulus was 200 GPa, its width was 20 mm, Poisson's ratio was 0.3, and the density was 7800 kg/m^3.

Table 2. Comparison of FE and RCSA natural frequency predictions.

L_1 (mm)	L_2 (mm)	t_1 (mm)	t_2 (mm)	FE f_n (Hz)	RCSA f_n (Hz)	% diff.
150	0	6	6	217.96	217.87	0.04
146	4	6	4	221.79	221.70	0.04
142	8	6	4	225.51	225.42	0.04
132	18	6	4	234.28	234.19	0.04
122	28	6	4	242.03	241.96	0.03
100	50	6	4	253.20	253.37	-0.07
75	75	6	4	248.22	249.26	-0.42
50	100	6	4	219.84	221.82	-0.90
25	125	6	4	180.46	182.63	-1.20
10	140	6	4	157.53	159.54	-1.28
0	150	4	4	145.39	145.34	0.03

The k_1 stiffness results from the rib's free end are presented in Table 3 and Fig. 3. The k_2 stiffness results from the location of the step change in rib thickness are provided in Table 4 and Fig. 4.

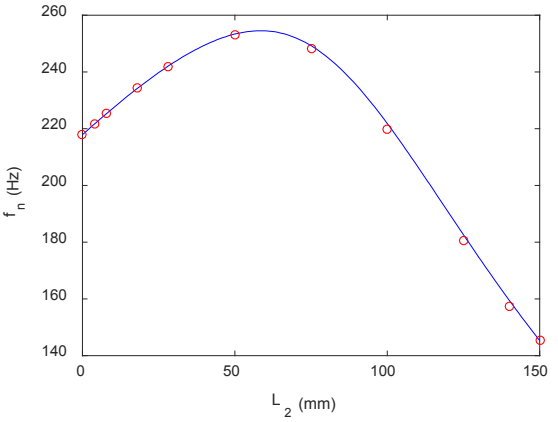

Fig. 2. Graphical comparison of FE (circles) and RCSA (line) natural frequency predictions.

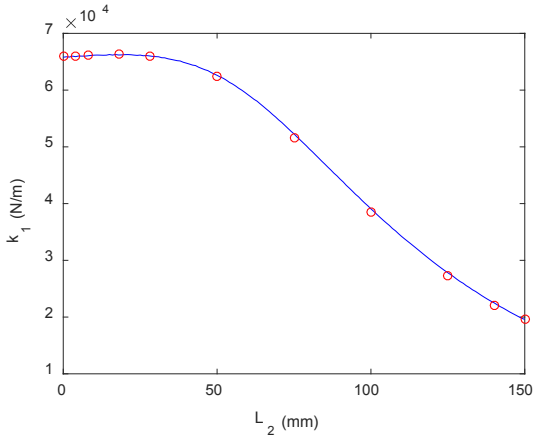

Fig. 3. Graphical comparison of FE (circles) and RCSA (line) k_1 stiffness predictions.

Table 3. Comparison of FE and RCSA k_1 stiffness predictions.

L_1 (mm)	L_2 (mm)	t_1 (mm)	t_2 (mm)	FE k_1 (N/m)	RCSA k_1 (N/m)	% diff.
150	0	6	6	6.5915×10^4	6.5758×10^4	0.24
146	4	6	4	6.6054×10^4	6.5894×10^4	0.24
142	8	6	4	6.6176×10^4	6.6016×10^4	0.24
132	18	6	4	6.6329×10^4	6.6185×10^4	0.22
122	28	6	4	6.6057×10^4	6.5969×10^4	0.13
100	50	6	4	6.2371×10^4	6.2577×10^4	-0.33
75	75	6	4	5.1665×10^4	5.2243×10^4	-1.12
50	100	6	4	3.8433×10^4	3.9059×10^4	-1.63
25	125	6	4	2.7277×10^4	2.7779×10^4	-1.84
10	140	6	4	2.2057×10^4	2.2471×10^4	-1.88
0	150	4	4	1.9537×10^4	1.9513×10^4	0.12

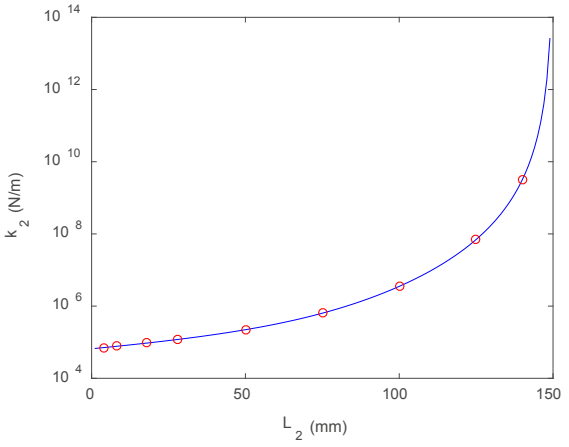

Fig. 4. Graphical comparison of FE (circles) and RCSA (line) k_2 stiffness predictions.

Table 4. Comparison of FE and RCSA k_2 stiffness predictions.

L_1 (mm)	L_2 (mm)	t_1 (mm)	t_2 (mm)	FE k_2 (N/m)	RCSA k_2 (N/m)	% diff.
150	0	6	6	-	-	-
146	4	6	4	7.1162×10^4	7.0989×10^4	0.24
142	8	6	4	7.7001×10^4	7.6811×10^4	0.25
132	18	6	4	9.4891×10^4	9.4646×10^4	0.26
122	28	6	4	1.1945×10^5	1.1912×10^5	0.28
100	50	6	4	2.2295×10^5	2.2184×10^5	0.50
75	75	6	4	6.4489×10^5	6.3670×10^5	1.27
50	100	6	4	3.6000×10^6	3.5204×10^6	2.21
25	125	6	4	7.1920×10^7	6.9920×10^7	2.78
10	140	6	4	3.2515×10^9	3.1501×10^9	3.12
0	150	4	4	-	-	-

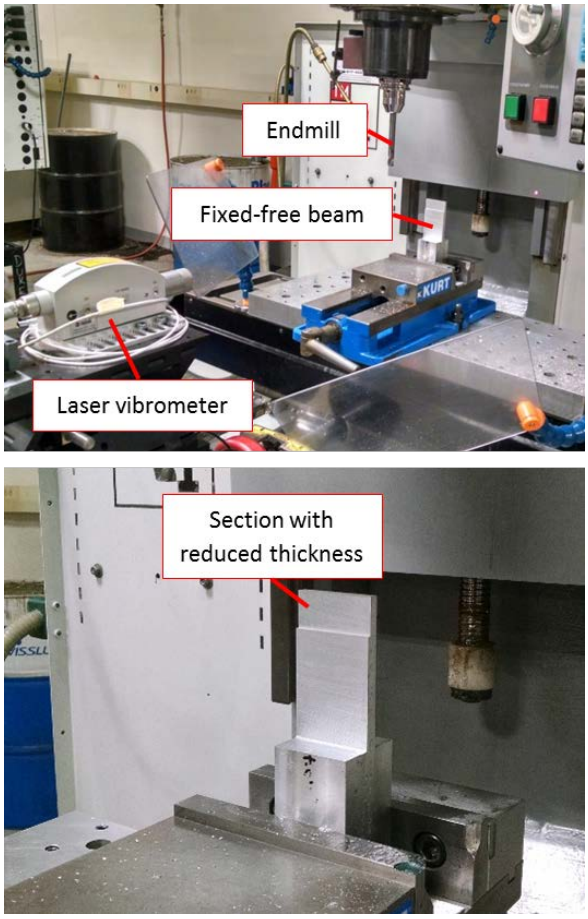

Fig. 5. Experimental setup. (Top) The fixed-free aluminum beam was mounted in a vise which was clamped to the machine table. The laser vibrometer was used to measure the beam response due to a force impact (applied by a modal hammer). (Bottom) The beam thickness was reduced over a section with a known length and receptance measurements were performed at the top and bottom of the section.

3. Experimental setup

Receptance measurements were completed using a modal hammer (PCB 086C04) to excite the beam and a laser vibrometer (Polytec OFV 5000 controller/OFV 534 laser head) to measure the velocity; see Fig. 5. The direct receptance measurements were performed at the aluminum beam's free end and at the change in thickness. The length of the reduced thickness section was changed by machining, where a 12.7 mm diameter three-flute

solid carbide endmill (approximately 100 mm stickout length) was used (0.1 mm/tooth, 3900 rpm). The beam thickness was removed in 10 mm axial steps with a final radial depth of 1 mm. The beam width was 44.96 mm. Measurements were performed after each machining pass.

4. Results

A comparison between experiments and RCSA receptances was completed for the fundamental bending mode of the aluminum beam displayed in Fig. 5. For the RCSA beams models, the assumed elastic modulus was 69 GPa, Poisson's ratio was 0.33, and the density was 2700 kg/m^3. Note that the modulus can vary depending on the machined surface texture [26-27]. The natural frequency results are displayed in Table 5 and Fig. 6. The k_1 stiffness results are presented in Table 6 and Fig. 7. The k_2 stiffness results are shown in Table 7 and Fig. 8. In all cases, the parameters were extracted from the measured receptances by modal fitting.

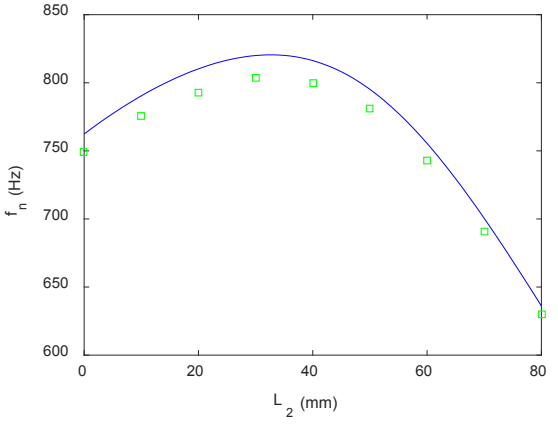

Fig. 6. Graphical comparison of experiments (squares) and RCSA (line) natural frequency predictions.

Table 5. Comparison of experiments and RCSA predictions for natural frequency.

L_1 (mm)	L_2 (mm)	t_1 (mm)	t_2 (mm)	Exp. f_n (Hz)	RCSA f_n (Hz)	% diff.
80	0	6	6	749	762.4	-1.78
70	10	6	5	776	790.39	-1.85
60	20	6	5	793	810.25	-2.18
50	30	6	5	804	820.04	-2.00
40	40	6	5	800	816.27	-2.03
30	50	6	5	781	795.15	-1.81
20	60	6	5	743	755.49	-1.68
10	70	6	5	691	700.45	-1.37
0	80	5	5	630	636.14	-0.97

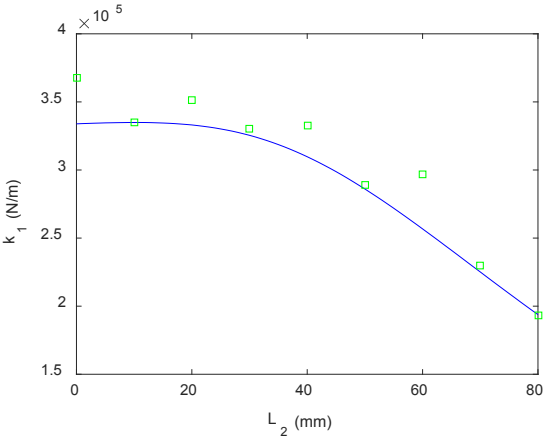

Fig. 7. Graphical comparison of experiments (squares) and RCSA (line) k_1 stiffness predictions.

Table 6. Comparison of experiments and RCSA predictions for stiffness k_1.

L_1 (mm)	L_2 (mm)	t_1 (mm)	t_2 (mm)	Exp. k_1 (N/m)	RCSA k_1 (N/m)	% diff.
80	0	6	6	3.68×10^5	3.34×10^5	9.27
70	10	6	5	3.35×10^5	3.35×10^5	0.04
60	20	6	5	3.51×10^5	3.33×10^5	5.12
50	30	6	5	3.30×10^5	3.25×10^5	1.38
40	40	6	5	3.33×10^5	3.10×10^5	6.99
30	50	6	5	2.89×10^5	2.86×10^5	1.03
20	60	6	5	2.97×10^5	2.57×10^5	13.6
10	70	6	5	2.30×10^5	2.25×10^5	2.14
0	80	5	5	1.93×10^5	1.94×10^5	-0.40

Table 7. Comparison of experiments and RCSA predictions for stiffness k_2.

L_1 (mm)	L_2 (mm)	t_1 (mm)	t_2 (mm)	Exp. k_2 (N/m)	RCSA k_2 (N/m)	% diff.
80	0	6	6	-	-	-
70	10	6	5	6.07×10^5	4.87×10^5	19.8
60	20	6	5	9.02×10^5	7.69×10^5	14.7
50	30	6	5	1.72×10^6	1.38×10^6	20.0
40	40	6	5	3.92×10^6	2.97×10^6	24.2
30	50	6	5	1.46×10^7	8.68×10^6	40.6

20	60	6	5	6.21×10^{7}	4.26×10^{7}	31.5
10	70	6	5	2.24×10^{8}	6.80×10^{8}	-203.5
0	80	5	5	-	-	-

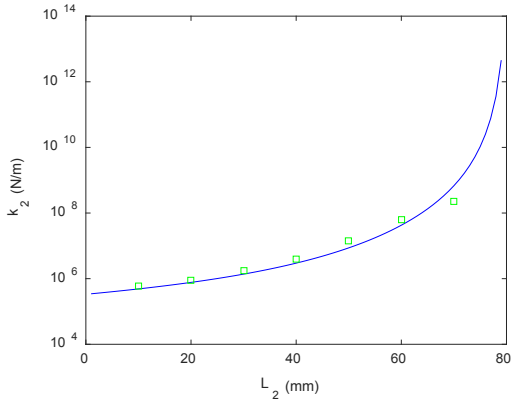

Fig. 8. Graphical comparison of experiments (squares) and RCSA (line) k_2 stiffness predictions (semilog scale).

In addition to the natural frequency and stiffness values, the dimensionless viscous damping ratios were also extracted from the measured direct receptances. These values are critical because first principle techniques for damping prediction are not available and the damping must, therefore, be included by the modeler based on experience or measurements. The results for the aluminum beam are displayed in Fig. 9 for all nine geometries; damping ratios were extracted from direct receptance measurements at both the free end and thickness change location. The average damping ratio is 0.28% with a standard deviation of 0.04%. The low damping for monolithic structures exacerbates the challenges associated with machining thin, near net shape ribs to produce the final thinner geometries.

In practice, the value of the results presented here is realized when incorporated into a pre-process operating parameter selection algorithm. Based on the machining path and subsequent material removal, the change in beam geometry and, therefore, dynamics can be predicted and the operating parameters can be appropriately selected. For example, using the predicted mass and stiffness together with an informed guess for the associated damping, the corresponding stability limit can be predicted for each machining pass [1]. As the stability limit changes with the beam dynamics, two options are available: 1) the operating parameters can be modified between passes to achieve maximum material removal rates; or 2) the minimum stability limit from all passes can be used to select one set of operating parameters that ensure stable performance throughout the material removal process.

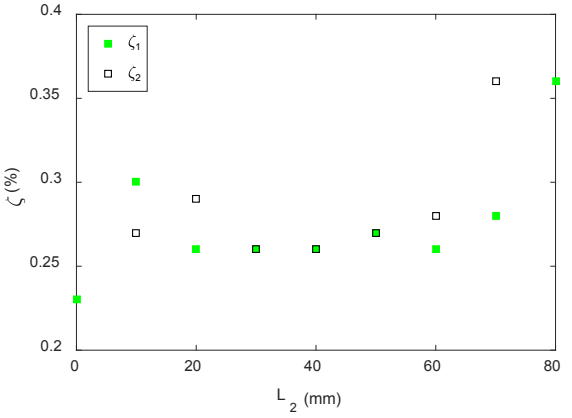

Figure 9: Experimental damping ratio values from measured direct receptances at the beam's free end, ζ_1, and at the location of the step change in thickness, ζ_2.

5. Conclusions

An analytical approach was presented for predicting thin rib, fixed-free beam dynamics with varying geometries. It was based on receptance coupling substructure analysis (RCSA). Comparison with finite element calculations showed that the RCSA approach provided good agreement when predicting the component receptances.

Experiments were also conducted to compare measured fixed-free beam receptances to RCSA predictions. An aluminum beam was machined between receptance measurements to change the thickness. The measured and predicted natural frequencies agreed with an average percent difference of -1.74% for the nine beam profiles. The measured and predicted stiffness values for the fundamental bending mode at the beam's free end agreed with an average percent difference of 4.35% for the nine beam profiles.

Acknowledgements

The authors thank Dr. John Ziegert for helpful discussions. They also gratefully acknowledge financial support from MAI BA-21 (USAF contract number FA8650-17-2-5246).

References

[1] Schmitz, T. and Smith, K.S., 2009, Machining Dynamics: Frequency Response to Improved Productivity, Springer, New York, NY.

[2] Budak, E., Altintas, Y., 1995, Modeling and avoidance of static form errors in peripheral milling of plates, International Journal of Machine Tools & Manufacture, 35: 459-476.

[3] Tlusty, J., Smith, S., and Winfough, W., 1996, Techniques for the use of long slender end mills in high-speed milling, Annals of the CIRP, 45/1: 393-396.

[4] Smith, S. and Dvorak, D., 1998, Tool path strategies for high speed milling aluminum workpieces with thin webs, Mechatronics, 8: 291-300.

[5] Ning, H., Zhigang, W., Chengyu, J., and Bing, Z., 2003, Finite element method analysis and control stratagem for machining deformation of thin-walled components, Journal of Materials Processing Technology, 139: 332-336.

[6] Ratchev, S., Nikov, S., and Moualek, I., 2004, Material removal simulation of peripheral milling of thin wall low-rigidity structures using FEA, Advances in Engineering Software, 35: 481-491.

[7] Ratchev, S., Liu, S., Huang, W., and Becker, A.A., 2004, Milling error prediction and compensation in machining of low-rigidity parts, International Journal of Machine Tools & Manufacture, 44: 1629-1641.

[8] Bravo, U., Altuzarra, O., López de Lacalle, L.N., Sánchez, J.A., and Campa, F.J., 2005, Stability limits of milling considering the flexibility of the workpiece and the machine, International Journal of Machine Tools & Manufacture, 45: 1669-1680.

[9] Ratchev, S., Liu, S., and Becker, A.A., 2005, Error compensation strategy in milling flexible thin-wall parts, Journal of Materials Processing Technology, 162-163: 673-681.

[10] Thevenot, V., Arnaud, L., Dessein, G., and Cazenave-Larroche, G., 2006, Influence of material removal on the dynamic behavior of thin-walled structures in peripheral milling, Machining Science and Technology, 10/3: 275-287.

[11] Mañé, I., Gagnol, V., Bouzgarrou, B.C., and Ray, P., 2008, Stability-based spindle speed control during flexible workpiece high-speed milling, International Journal of Machine Tools & Manufacture, 48: 184-194.

[12] Rai, J.K. and Xirouchakis, P., 2008, Finite element method based machining simulation environment for analyzing part errors induced during milling of thin-walled components, International Journal of Machine Tools & Manufacture, 48: 629-643.

[13] Seguy, S., Dessein, G., and Arnaud, L., 2008, Surface roughness variation of thin wall milling, related to modal interactions, International Journal of Machine Tools & Manufacture, 48: 261-274.

[14] Adetoro, O.B., Wen, P.H., Sim, W.M., and Vepa, R., 2009, Stability lobes prediction in thin wall machining, Proceedings of the World Congress on Engineering 2009 Vol I, WCE 2009, July 1-3, 2009, London, UK.

[15] Chen, W., Xue, J., Tang, D., Chen, H., and Qu, S., 2009, Deformation prediction and error compensation in multilayer milling processes for thin-walled parts, International Journal of Machine Tools & Manufacture, 49: 859-864.

[16] Gang, L., 2009, Journal of Materials Processing Technology, Study on deformation of titanium thin-walled part in milling process, 209: 2788-2793.

[17] Arnaud, L., Gonzalo, O., Seguy, S., Jauregi, H., and Peigné, G., 2011, Simulation of low rigidity part machining applied to thin-walled structures, International Journal of Advanced Manufacturing Technology, 54: 479-488.

[18] Izamshah, R., Mo, J.P.T , and Ding, S., 2011, Hybrid deflection prediction on machining thin-wall monolithic aerospace components, Proc. IMechE Part B: Journal of Engineering Manufacture, 226: 592-605.

[19] Smith, S., Wilhelm, R., Dutterer, B., Cherukuri, H., and Goel, G., 2012, Sacrificial structure preforms for thin part machining, CIRP Annals - Manufacturing Technology, 61: 379-382.

[20] Polishetty, A., Goldberg, M., Littlefair, G., Puttaraju, M., and Patil, P., 2014, A preliminary assessment of machinability of titanium allow Ti 6Al 4V during thin wall machining using trochoidal milling, Procedia Engineering, 97: 357-364.

[21] Schmitz, T. and Smith, K.S., 2012, Mechanical Vibrations: Modeling and Measurement, Springer, New York, NY.

[22] Bishop, R.E.D., and Johnson, D.C., 1960, The Mechanics of Vibration, Cambridge University Press, Cambridge, UK.

[23] Weaver, Jr., W., Timoshenko, P., and Young, D., 1990, Vibration Problems in Engineering, 5th Ed., John Wiley and Sons, New York, NY.

[24] Schmitz, T. and Duncan, G.S., 2005, Three-component receptance coupling substructure analysis for tool point dynamics prediction, Journal of Manufacturing Science and Engineering, 127/4: 781-790.

[25] Hutchinson, J., 2001, Shear coefficients for Timoshenko beam theory, Journal of Applied Mechanics, 68: 87-92.

[26] Olsen, R.H. and Moreen, H.A., 1973, Calculation of the elastic anisotropy of Ti:6Al-4V alloy sheet from pole figure data, Matellurgical Transactions, 4: 701-705.

[27] Kamaya, M., 2009, A procedure for estimating Young's modulus of textured polycrystalline materials, International Journal of Solids and Structures, 46: 2642-2649.